CHARACTERIZATION OF ON-HUMAN-BODY UWB RADIO PROPAGATION CHANNEL

Y. P. Zhang, Li Bin, and Cao Qi
School of Electrical and Electronic Engineering, Nanyang Technological University, Nanyang Avenue, Singapore

Received 11 November 2006

ABSTRACT: *Wireless body area network (WBAN) has begun to receive attention recently. Ultra wideband (UWB) is a promising technology for WBAN applications. This article presents the results of UWB radio channel measurements performed on human bodies from 3.1 to 10.6 GHz in indoor environments. The measurements were devised to generate the radiographs of path loss and delay spread for the first time. The radiographs contain both qualitative and quantitative information on the channel. They clearly display the influence of the body on the channel and thus reveal where the network nodes should be strategically placed on the body in the design of the UWB WBAN systems. They directly give such channel parameters as path loss and delay spread. They also reflect variations of the channel on and in close proximity to the body. In addition, the measurements were made in an anechoic chamber to expose the impact of the body and to study the effect of different environments on the channel. It is shown that for the UWB channel on the body the path loss exponent* $n = 2.7$ *can be used, while for the UWB channel through the body the path loss exponent increases to* $n = 3.7$. *The maximum value of the rms delay spread is 12 ns. The rms delay spread values are less than 6 ns 50% of the time. The number of multipath components increases with the separation between transmit and receive antennas. Because of the nonreflecting mechanism, the path loss is larger and the delay spread is smaller in the anechoic chamber environment.* © 2007 Wiley Periodicals, Inc. Microwave Opt Technol Lett 49: 1365–1371, 2007; Published online in Wiley InterScience (www.interscience.wiley.com). DOI 10.1002/mop.22411

Key words: *UWB antenna; UWB propagation; wireless body area network*

1. INTRODUCTION

A BAN is a network with its nodes placed close to the body on or in everyday clothing [1]. The BAN topology comprises master and slave sensor nodes. A master node is for both transmission and reception. The master node has a somewhat higher complexity and faster computational capability to provide support for higher date rates. A hand phone can be configured to be a master node. A slave node is for either transmission or reception only. The slave node must be small, simple, low cost, and energy efficient. A good example of the slave node is a hearing aid.

A wireless body area network (WBAN) employs wireless technology to realize the connectivity between a master and a slave node [2, 3]. The WBAN has some distinct features and special requirements. Because of the close proximity of the network to the body, the WBAN must fit the shape of the human body and limit radiation power from the transmit nodes to extremely low level to reduce potential hazards. Thus, the data transmission from a slave node to a master node may need multiple hops.

A ultra wideband (UWB) radio operates in the frequency range from 3.1 to 10.6 GHz. The mean transmit power must not exceed −41 dBm/MHz [4]. The UWB radio is a promising technology for WBAN applications. In this article, we characterize the UWB radio channel on the human body by measurements. The measurements were devised to generate the radiographs of path loss and delay spread for the first time. The channel parameters as path loss and delay spread are extracted and the statistical distributions of the channel variations are determined from the radiographs.

A UWB channel measurement was conducted for wireless personal area network (WPAN) applications [5]. The effect of the body on UWB signal propagation in an indoor environment was measured for one antenna placed on the body and the other antenna kept away from the body. There are only a few articles that report channel measurements and modeling with both transmit and receive antennas placed on the body for WBAN applications [6–11]. Zasowski et al. measured the on-human-body channel in an office room and an anechoic chamber in the frequency range of 3–6 GHz [6]. They extracted channel parameters such as path loss and delay spread from the measurements and highlighted the influence of the human body on channel characteristics. Alomainy et al. measured the on-human-body channel in an anechoic chamber in the frequency range of 3–9 GHz [7]. They evaluated the consequences of changes in body postures and positions on channel characteristics and demonstrated the effects of different antennas on such channel parameters as path loss and delay spread. Fort et al. proposed a simple statistical model for evaluating WBAN systems [8]. Very similar work as in Ref. 8 also can be found in Ref. 9. Hao et al. measured the on-human-body channels at 2.4 GHz and modeled it by the Finite-difference time-domain (FDTD) method [10]. Kamarudin et al. measured the on-human-body channels at 2.4 GHz with an emphasis on the optimum choice of antennas [11]. Review of these studies shows that no measurement and modeling that cover the whole UWB band from 3.1 to 10.6 GHz has been made. Also, the reported channels were all sparsely sounded on a few predefined points. The important statistical characteristics of the channels had to be extracted from the limited FDTD simulations [8, 9]. Considering that a human body has a finite size, we conducted channel measurements on and in close proximity to the body at a much higher resolution. The sampling distance was set to be 2 cm, which is shorter than the shortest wavelength. We believe that these measurements represent the most extensive set of publicly reported measurements taken to characterize on-human-body UWB radio channel.

The goal of this large measurement campaign is threefold: (1) accurately measure the channel to generate the radiographs of path loss and delay spread for the first time; (2) reveal the influence of the human body on the channel; (3) provide practical values of statistical channel parameters for the design of the UWB WBAN systems. Section 2 describes the measurements. Definitions of the statistical parameters are presented in Section 3.1. and the measurement results are analyzed and discussed in Section 3.2. Section 4 summarizes the conclusions.

2. DESCRIPTION OF MEASUREMENTS

Radio propagation channel measurements have always been recognized as having an important part to play in the development of complex wireless area networks. This is particularly true for ultra wideband (UWB) radio [12–14].

2.1. Measurement Setup

The measurement setup is shown in Figure 1. The key component of the setup is the 40 GHz HP network analyzer. The antennas used in the measurements were two planar monopoles. They were designed, constructed, and tested in our antenna laboratory. Figure 2 shows the measured antenna return loss on and off the human body. As shown, the antenna return loss is above −10 dB from 3.1 to 3.5 GHz and is below −10 dB from 3.5 to 10.6 GHz for the off-body case. The antenna return loss is improved to below −10 dB for the on-body case over the entire UWB band. This is due to the lossy nature of the body. Figure 3 shows the measured antenna far-field radiation patterns for both E- and H-planes at the UWB

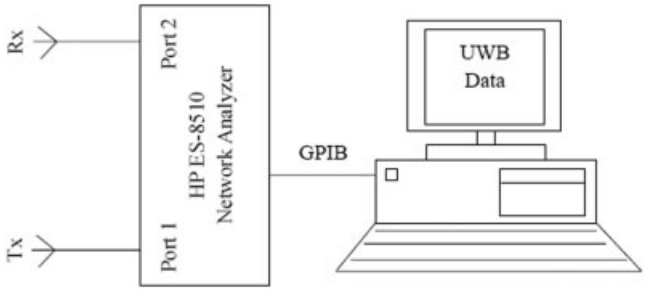

Figure 1 The measurement setup

central frequency 6.85 GHz. It is seen that the antenna has an omni directional radiation pattern in the E-plane and a ∞ shaped radiation pattern in the H-plane. It is known that the antenna radiation patterns will change when it is placed on the body. Unfortunately, the change cannot be measured with our testing facilities.

The setup can measure the transfer function of the channel. The amplitude loss and phase shift of each frequency component caused by the channel is recorded. Moreover, the impulse response of the channel can be obtained by taking the inverse Fourier transform. The bandwidth capability of the setup permitted UWB channel measurement over the frequency range of 3.1–10.6 GHz. With 4.6875 MHz steps, corresponding to 1601 frequency components, we could detect a multipath with a time delay up to 213 ns. This detectable range is suitable for indoor environments [15]. The time domain resolution corresponds to the ability to resolve two closely spaced responses. There are abrupt transitions in a frequency domain measurement at the start and stop frequencies, which cause overshoot and ringing in the time domain response. The frequency domain windowing can smoothen the abruptness of the frequency domain transitions but at the cost of the time domain resolution. For UWB channel sounding, the time domain resolution is important and critical due to narrow pulses, consequently, a minimum window is desirable [13]. Using the minimum window, one can find the time domain resolution to be 160 ps.

2.2. Measurement Site

The measurements were conducted on the Nanyang University campus in a staff lounge room and an anechoic chamber. The staff lounge room is located on the third floor (level B4 by the NU convention) of building S2.2. The building is a six-story concrete

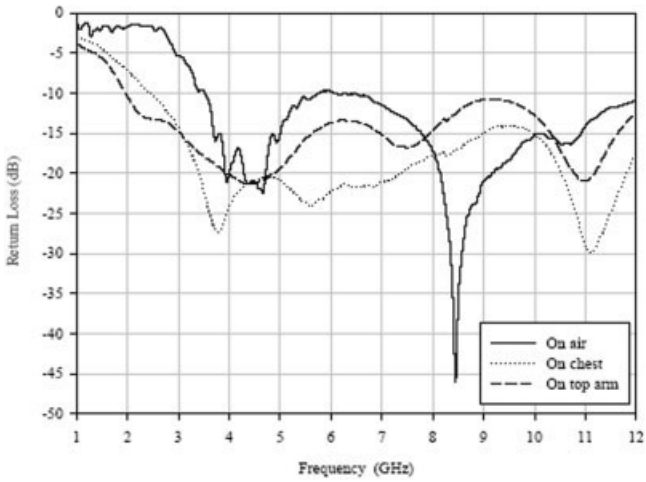

Figure 2 The antenna and its measured return loss

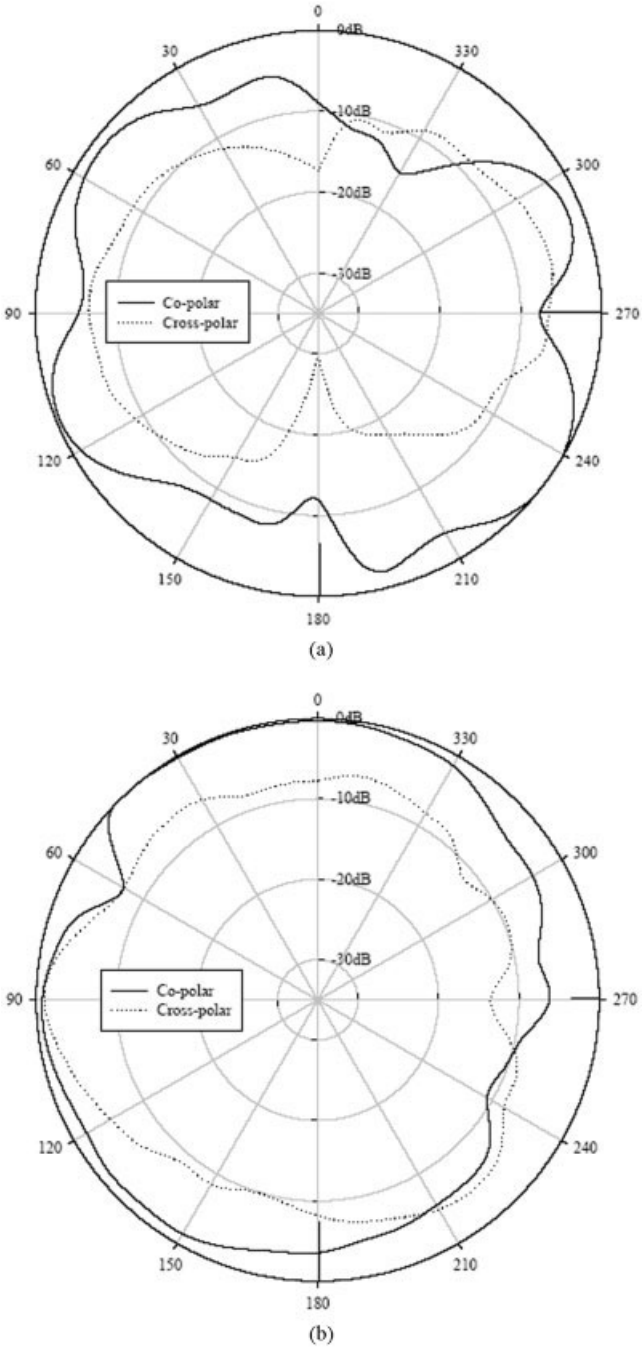

Figure 3 The antenna measured radiation patterns: (a) E-plane and (b) H-plane

complex, which was built in 2003. Figure 4 shows the photo of the staff lounge room. Three arched sofas, one cabinet, a 34-inch plasma TV, and a desktop computer could not be taken into the photo. The room dimensions are $8 \times 8 \times 4$ m^3. In this section, all the dimensions are given in the order of length, width, and height.

The anechoic chamber is located on the second floor (level B5 by the NU convention) of building S2. The building is a six-story concrete complex, which was built in 1991. Figure 5 shows the photo of the anechoic chamber. The anechoic chamber was built to characterize small antennas from 2 to 50 GHz. The dimensions of the anechoic chamber are $4 \times 3 \times 3$ m^3. The main rationale of choosing the staff lounge room and the anechoic chamber was to

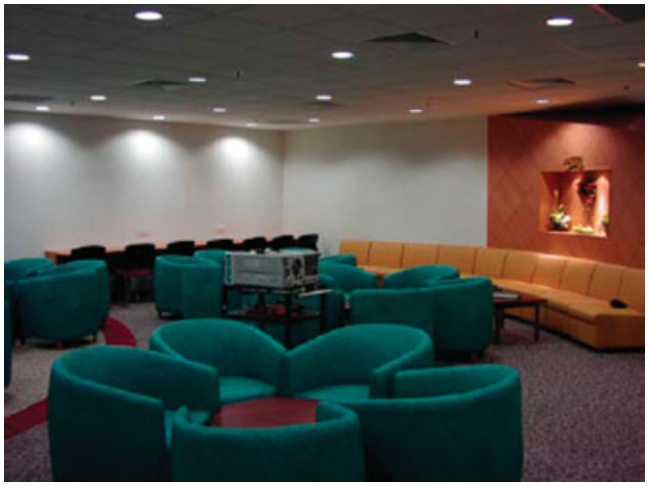

Figure 4 The photo of test room. [Color figure can be viewed in the online issue, which is available at www.interscience.wiley.com]

investigate the influence of the environment and to expose the impact of the body on the channel.

2.3. Measurement Procedure

To measure the channel, three people of different heights (1.65, 1.70, 1.75 m) and weights (55, 60, 65 kg) were selected. The measurements were made on or in close proximity to each body. During the measurements, the people under test was to stand straight and upright at a fixed location, and the transmit antenna was placed on the right upper arm near the shoulder. The transmit antenna placed there was because a longer path and a better safety are offered. Figure 6 shows the defined points to generate the radiographs of path loss and delay spread. The receive antenna was moved to the points to collect the data. At the points, the receive antenna was carefully oriented to minimize the polarization loss with respect to the transmit antenna.

3. STATISTICAL PARAMETERS OF THE CHANNEL

Statistical parameters characterize general channel properties that are useful for system design and modulation analysis. This section presents definitions of the statistical parameters and the analysis of the measurement results.

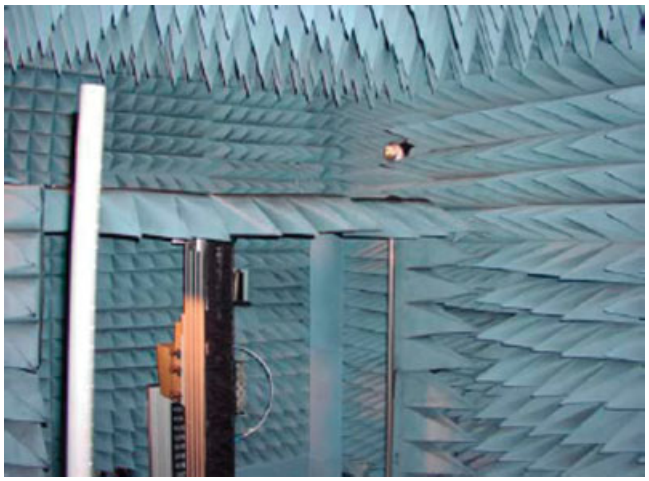

Figure 5 The photo of chamber room. [Color figure can be viewed in the online issue, which is available at www.interscience.wiley.com]

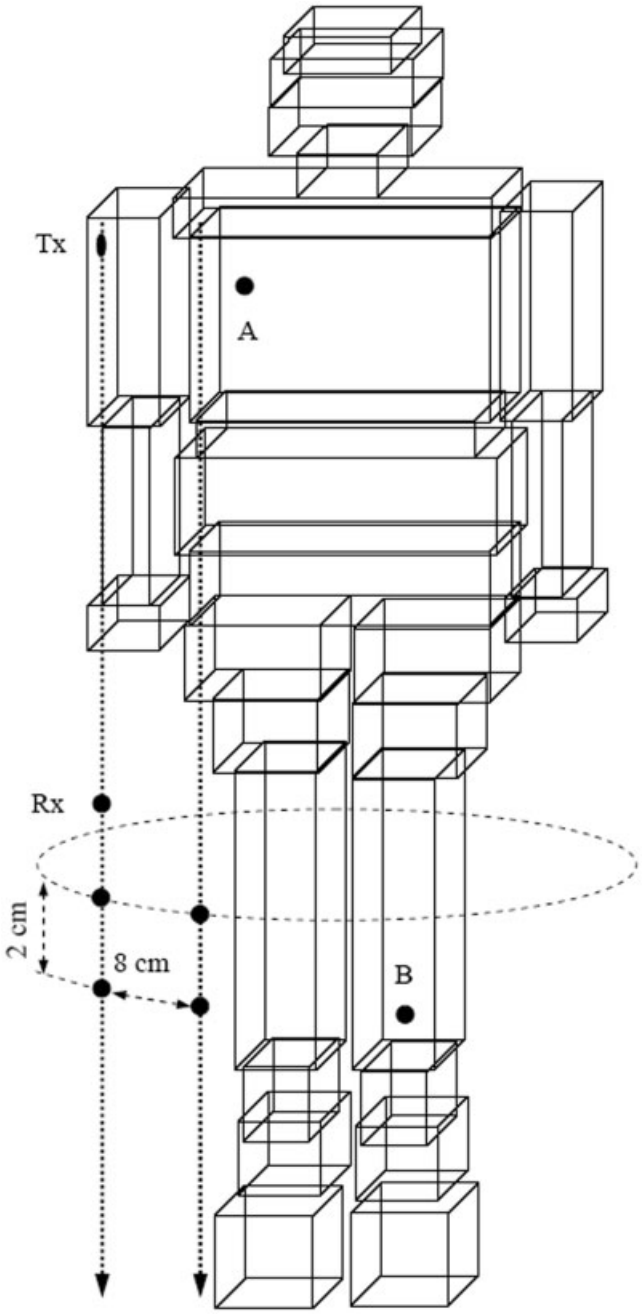

Figure 6 Test point locations

3.1. Definitions of the Statistical Parameters

3.1.1. Path Loss. Path loss describes the signal power loss from the transmit antenna to the receive antenna. Path loss does not depend on the antenna gains or the transmitted power levels. The average path loss can be directly calculated from the measured transfer function of the channel as

$$\mathrm{PL}(d) = 10 \log_{10}\left[\frac{1}{MN}\sum_{j=1}^{M}\sum_{i=1}^{N}\left|H_j^d(f_i)\right|^2\right], \qquad (1)$$

where H_j^d denotes the jth transfer function of the channel at a frequency f_i in a distance d, M is the number of transfer functions for the distance d, and N is the number of frequency components

in the transfer function of the channel [6, 8]. The average path loss can be expressed as

$$\mathrm{PL}(d) = \mathrm{PL}_o + 10n \log_{10}\left(\frac{d}{d_0}\right) + X_\sigma, \tag{2}$$

where PL_0 is the path loss at the close-in reference distance d_0, n is the path loss exponent, and X_σ is the shadowing fading in dB. We set d_0 to be 1 m for better comparison with available results and find the values for PL_0, n, and X_σ from Eq. (1). Note that an exponential path loss model mainly based on the FDTD simulations is presented in Ref. 9 for wireless body area network (WBAN) system design. It is found that the exponential path loss model only provides a good fit to the data at close range for $d <$ 10 cm [8]. Therefore, we do not use it to fit our data.

3.1.2. Delay Spread. Delay including mean excess delay τ and rms delay spread τ_{rms} describes the time dispersion of a multipath channel. The mean excess delay can be used to estimate the search range of rake receivers and the rms delay spread can be used to determine the maximum data transmission rate in the channel without equalization. The mean excess delay τ and τ_{rms} delay spread can be obtained from an impulse response as follows: the impulse response $h(p,\tau)$is actually a power delay profile obtained from measurement point p and scaled such that the first wave arrives at $\tau = 0$ in the profile. The mean excess delay τ or the first moment of the power delay profile with respect to the first arriving wave is given by

$$\tau = \frac{\sum_{k=1}^{K} \tau_k h(p,\tau_k)}{\sum_{k=1}^{K} h(p,\tau_k)}. \tag{3}$$

The root mean square delay spread τ_{rms} is the square root of the second central moment of the power delay profile and expressed as

$$\tau_{\mathrm{rms}} = \sqrt{\frac{\sum_{k=1}^{K} \tau_k^2 h(p,\tau_k)}{\sum_{k=1}^{K} h(p,\tau_k)} - (\tau)^2}. \tag{4}$$

Strong echoes with long delays contribute significantly to τ_{rms}.

3.1.3. Number of Paths. A rake receiver may not be able to exploit closely spaced multipaths. It is of interest to generate statistics of the number of paths below the maximum achievable time resolution. It was mentioned that the time resolution is reduced with windowing, so we need a methodology for the reduction. The methodology is known as binning [13]. It is described as follows: first upsample the impulse response vector $h(p,\tau)$ by 20, then parse the upsampled $h(p,\tau)$ into sets pf points with desired time resolution, and finally calculate the sample for the lth bin as

$$h_l(p,\tau) = \sqrt{\sum_q |h(p,\tau)|^2}. \tag{5}$$

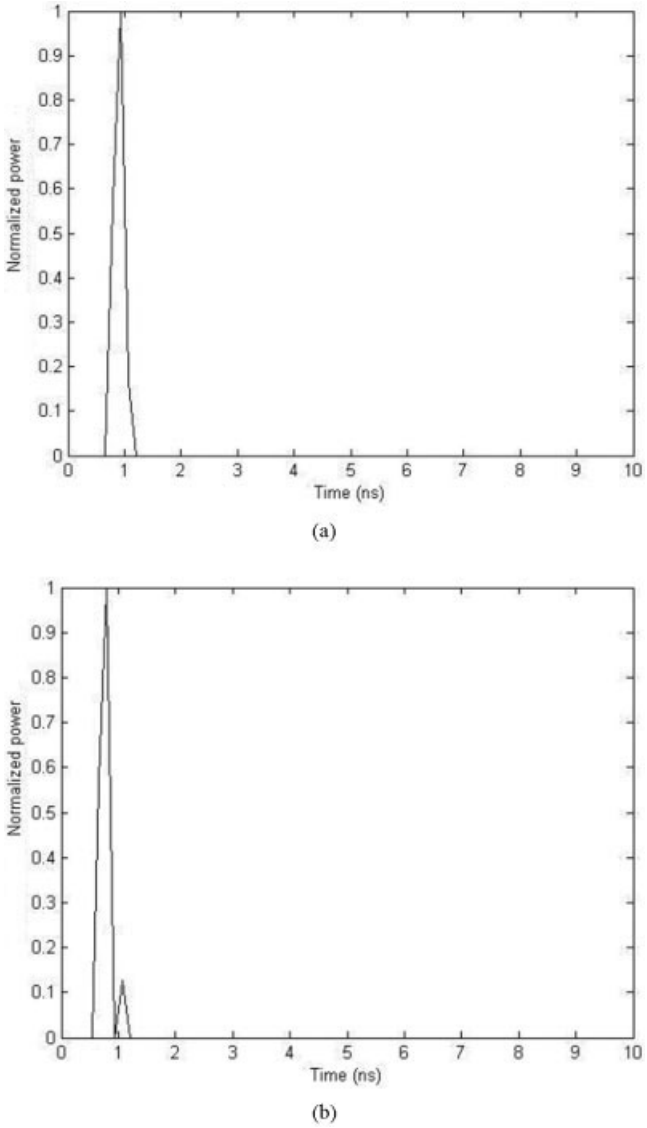

Figure 7 Received signals at point 1 in both anechoic chamber (a) and staff lounge room (b)

The number of paths can differ due to multipaths being binned into one path. The number of paths also depends on the threshold levels.

3.2. Results of Measured Statistical Parameters

A total of 2930 frequency transfer functions were recorded of which 2730 were recorded in the staff lounge room and 200 in the anechoic chamber. Each frequency transfer function consists of 1601 frequency points. Channel impulse responses are computed by an inverse Fourier transform.

Figure 7 shows normalized channel impulse responses measured at test point A in both anechoic chamber and staff lounge room. There is only one pulse for the channel impulse response measured in the anechoic chamber. This pulse comes from the line-of-sight (LOS) path. There are two pulses for the channel impulse response measured in the staff lounge room. The first pulse comes from the LOS path and the second from the reflected path due to the sizable network analyzer. Figure 8 shows normalized channel impulse responses measured at test point B in both anechoic chamber and staff lounge room. There are many pulses

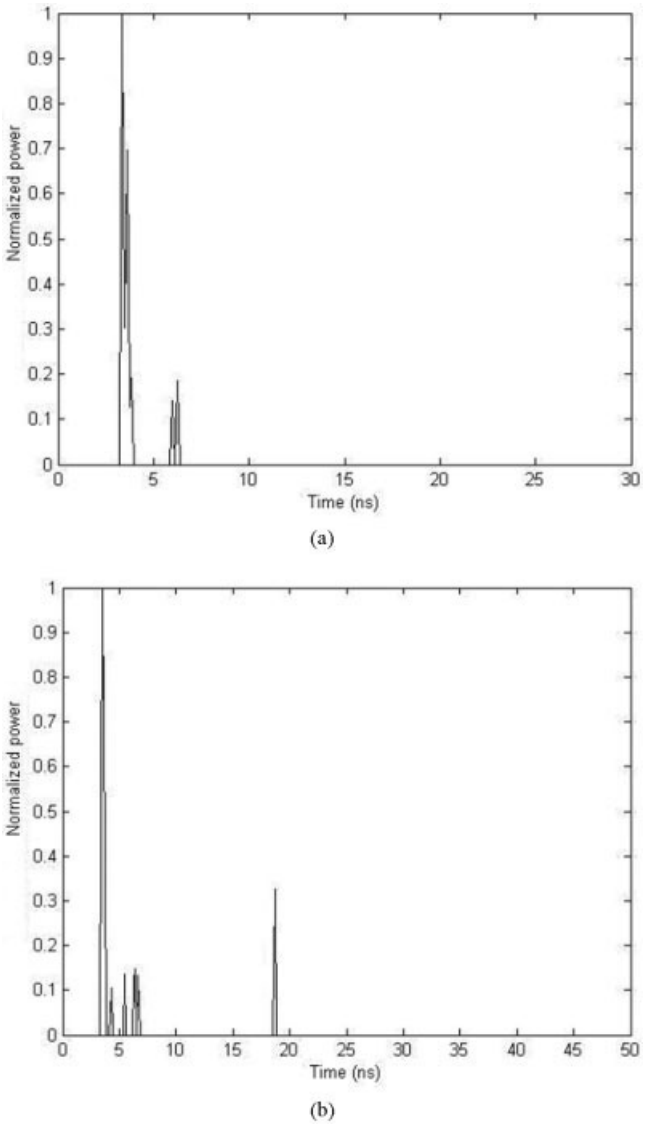

Figure 8 Received signals at point 23 in both anechoic chamber (a) and staff lounge room (b)

for the channel impulse response measured in the anechoic chamber. These pulses come from the direct and diffracted paths of the human body and perhaps some reflected paths from the antenna stand. There are even more pulses for the channel impulse response measured in the staff lounge room. The additional pulses originate from the reflected paths due to the walls, ceiling, and floor.

Figure 9 shows the radiograph of channel path loss on and in close proximity to the body in an unfolded format. The radiograph is generated from the Matlab calculation of Eq. (1) based on the channel transfer functions measured in the staff lounge room. It clearly shows the qualitative information on the channel: for example, where are LOS and non-LOS (NLOS) regions? The LOS region is located at the top two corners in the radiograph, which is mainly the side of the body near the transmit antenna. The NLOS region is located from the top to bottom middle part of the radiograph, which is mainly the other side of the body away from the transmit antenna. The radiograph also contains quantitative information on the channel. The channel path loss model parameters such as PL_0, n, and X_σ defined in Eq. (2) can be extracted from it by performing a least square fit computation. For the front

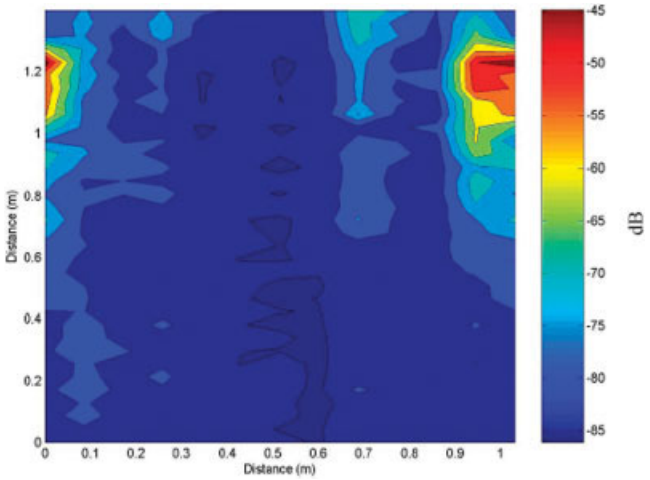

Figure 9 Path loss radiograph. [Color figure can be viewed in the online issue, which is available at www.interscience.wiley.com]

side of the body: It is found that (PL_0, n) is (−101 dB, 3.7), (−82 dB, 2.6), and (−86 dB, 2.2) for the horizontal, vertical, and diagonal routes, respectively. For the back side of the body: It is found that (PL_0, n) is (−93 dB, 2.8), (−82 dB, 2.9), and (−84 dB, 2.7) for the horizontal, vertical, and diagonal routes, respectively. Path loss exponents given in [6] are 4.1 and 2.7 for the horizontal and vertical routes, respectively. They are quite closed to our results 3.7 and 2.6. Note that the larger path loss exponent for the horizontal route is because of the transmission through the human body. The horizontal route can be considered as the most difficult propagation path for the WBAN channel.

Figure 10 shows the radiograph of channel rms delay spread on and in close proximity to the body in an unfolded format. The radiograph is generated from the Matlab calculation of Eqs. (3) and (4) based on the channel impulse responses obtained from inverse Fourier transform of the frequency transfer functions measured in the staff lounge room. To calculate τ and τ_{rms} from a channel impulse response, one has to give careful consideration to the threshold level. Usually, the threshold level is set to be 30 dB down from the peak in the studies of radio propagation channels for cellular radio or wireless local area network applications. Here

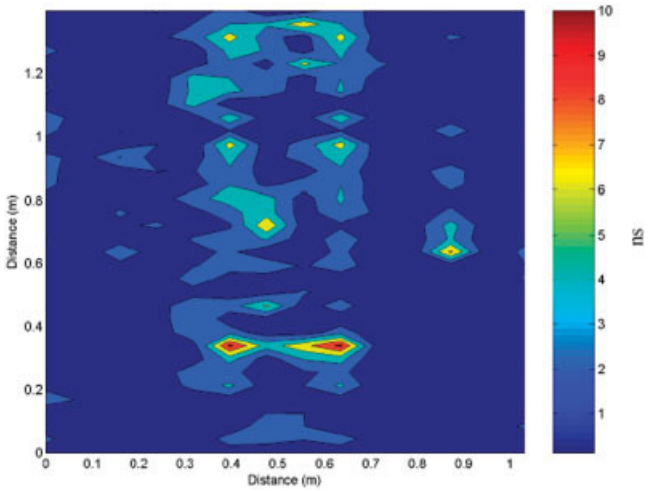

Figure 10 RMS delay spread radiograph. [Color figure can be viewed in the online issue, which is available at www.interscience.wiley.com]

another approach is adopted. We consider a 100 ns interval of the channel impulse response to calculate τ and τ_{rms}. This is because echoes from obstacles fade away after this time for WBAN applications. The radiograph of channel rms delay spread contains both qualitative and quantitative channel information. As can be seen, the rms delay spread τ_{rms} is larger in the NLOS region and smaller in the LOS region. In Matlab environment, the τ_{rms} value can be read directly from the radiograph. Since the rms delay spread values were not normally distributed, it was necessary to employ nonparametric statistical analysis. The statistics of the rms delay spread were compiled. The maximum value of the rms delay spread is 12 ns. The rms delay spread values are less than 6 ns 50% of the time. It is well known that performance of wireless communications systems operating in multipath environments is very sensitive to rms delay spread values. Simulation studies have shown that without diversity or equalization, the ratio of the rms delay spread to symbol duration in digital transmission must be kept below 0.2 to have a tolerable intersymbol interference [13]. On the basis of this criterion, the UWB on-human-body channel has a broad coherent bandwidth and can support the data rate up to 1.6 gigabits per second.

A rake receiver collects the energy in the multipath components of the channel. The complexity of the rake receiver increases with the number of its fingers which correspond to the number of multipath components that can be collected. Therefore, the distribution of the multipath components in the channel impulse responses is of particular interest [6]. Figure 11 shows the cumulative energy of the L strongest paths for the separation distances of 15 and 85 cm between transmit and receive antennas. As can be seen, if the rake receiver is designed to collect 80% of the whole energy; the rake receiver should have five fingers for the separation of 15 cm and 20 fingers for the separation of 85 cm.

Finally, we compare the path loss and rms delay spread between the anechoic chamber and the staff lounge room in Figure 12. It is evident from the figure that the path loss is higher and the rms delay spread is smaller in the anechoic chamber than those in the staff lounge room, which is the direct consequence of the non-reflecting mechanism in the anechoic chamber environment.

4. CONCLUSIONS

We presented the results of characterization of UWB radio propagation channel based on measurements performed on human bodies from 3.1 to 10.6 GHz in indoor and anechoic chamber environments. The measurements were devised to generate the radiographs of path loss and delay spread for the first time. The radiographs display the influence of the body on the channel and reflect variations of the channel on and in close proximity to the body; therefore, they are very useful in the design of the UWB WBAN systems. The channel parameters such as path loss and delay spread can be directly read from the radiographs. The results revealed that for the UWB channel on the body a path loss exponent $n = 2.7$ could be used, while for the UWB channel through the body the path loss exponent increased to $n = 3.7$. The maximum value of the rms delay spread was 12 ns. The rms delay spread values were less than 6 ns 50% of the time. The number of multipath components increased with the separation between transmit and receive antennas. Due to the nonreflecting mechanism, the path loss is larger and the delay spread is smaller in the anechoic chamber environment.

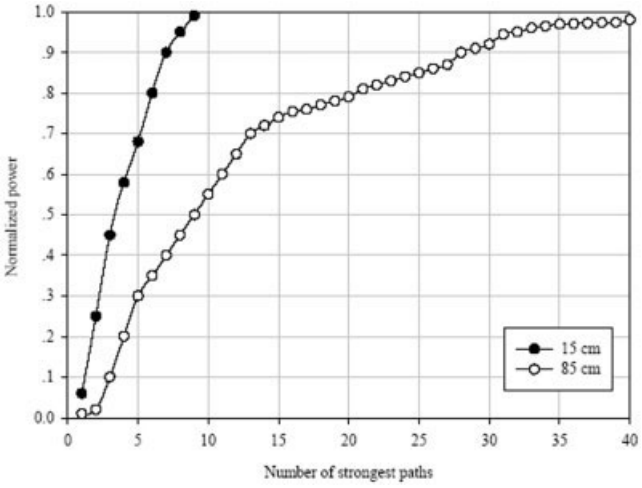

Figure 11 Cumulative normalized power of the L paths with the highest power in the staff lounge room

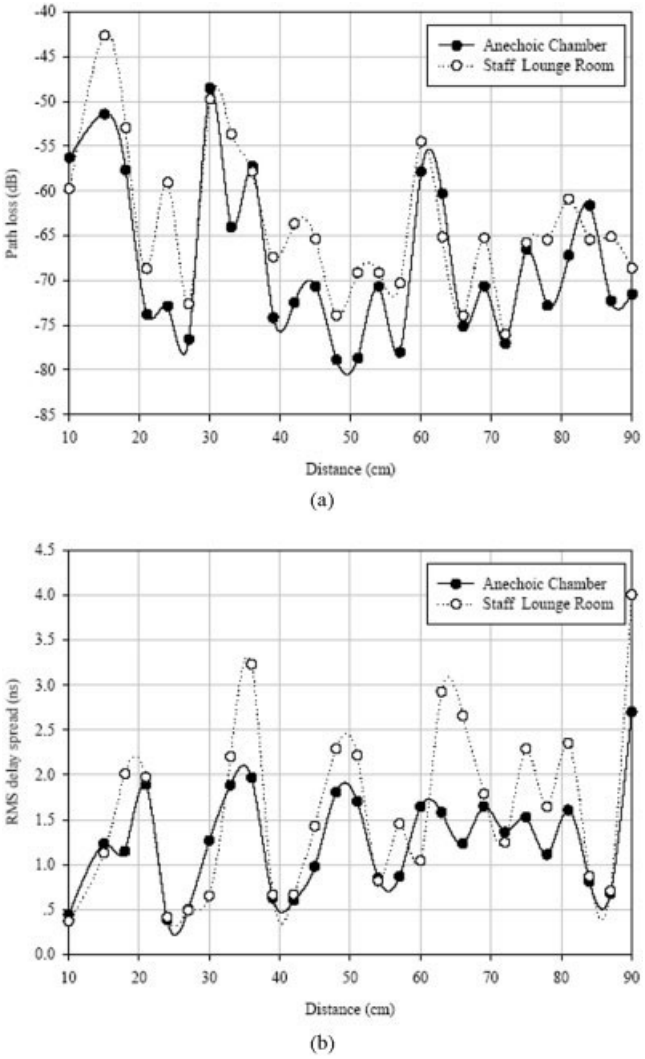

Figure 12 Comparison between the anechoic chamber and the staff lounge room: (a) path loss and (b) rms delay spread

ACKNOWLEDGMENTS

The author would like to thank L. L. Lee, Y. H. Chong, X. G. Gan, W. D. Leck, Y. M. Lim, W. K. Ng, K. L. Tan, Y. K. Tham, W. K. Chua, and C. T. Chong for their great assistance in the measurement campaign and data analysis.

REFERENCES

1. Wireless world research forum: Book of visions, 2001.
2. D. Marculescu, R. Marculescu, S. Park, and S. Jayaraman, Ready to ware, IEEE Spectrum 40 (2003), 28–32.
3. E. Jovanov, A. O'Donnell Lords, D. Raskovic, P.G. Cox, R. Adhami, and F. Andrasik, Stress monitoring using a distributed wireless intelligent sensor system, IEEE Eng Med Biol Mag 22 (2003), 49–55.
4. D. Porcino and W. Hirt, Ultra-wideband radio technology: Potential and challenges ahead, IEEE Commun Mag 41 (2003), 66–74.
5. T.B. Welch, R.L. Musselman, B.A. Emessiene, P.D. Gift, D.K. Choudhury, DN. Cassadine, and S.M. Yano, The effects of human body on UWB signal propagation in an indoor environment, IEEE J Select Areas Commun 20 (2002), 1778–1782.
6. T. Zasowski, F. Althaus, M. Stager, A. Wittneben, and G. Troster, UWB for noninvasive wireless body area networks: Channel measurements and results, IEEE Conf Ultra Wideband Sys Technol 1 (2003), 285–289.
7. A. Alomainy, Y. Hao, C.G. Parini, and P.S. Hall, On-body propagation channel charateristics for UWB wireless body-centric networks, In the conference of IEEE AP-S International Symposium on Antennas and Propagation and USNC/URSI National Radio Science Meeting, Washington DC, USA, 2005.
8. A. Fort, C. Desset, J. Ryckaert, P.D. Doncker, L.V. Biesen, and S. Donnay, Ultra wide-band body area channel model, In IEEE International Conference on Communications, Seoul, Korea, 2005.
9. http://grouper.ieee.org/groups/802/15/pub/04/.
10. Y. Hao, A. Alomainy, W. Song, C.G. Parini, P.S. Hall2, Y. Nechayev, and C.C. Constantinou, Numerical modeling of on-body radio propagation channel, In the IEEE Symposium on Antennas and Propagation, USA, 2005.
11. M.R. Kamarudin, Y.I. Nechayev, and P.S. Hall, Antenna for on-body communication systems, In the IEEE Workshop on Antenna Technology, Singapore, 2005.
12. J. Keignart and N. Daniele, Subnanosecond UWB channel sounding in frequency and temporal domain, IEEE Conf Ultra Wideband Sys Technol, 1 (2002), 25–30.
13. L. Rusch, C. Prettie, D. Cheung, Q.H. Li, and M. Ho, Characterization of UWB propagation from 2 to 8 GHz in a residential environment, Available at www.intel.com/technology/ultrawideband/downloads/ChannelJSAC02subLR.pdf.
14. A.F. Molisch, J.R. Foerster, and M. Pendergrass, Channel models for ultrawideband personal area networks, IEEE Wireless Commun 10 (2003), 14–21.
15. Y.P. Zhang and F. Wang, Time delay characteristics of in-room UHF radio channels, Microwave Opt Technol Lett 33 (2002), 115–119.

PERMITTIVITY CHARACTERIZATION FROM OPEN-END MICROSTRIP LINE MEASUREMENTS

J. Hinojosa
Universidad Politécnica de Cartagena, Departamento de Electrónica, Tecnología de Computadoras y Proyectos, Plaza del Hospital n°1, 30202 Cartagena (Murcia) –SPAIN

Received 13 Nov 2006

ABSTRACT: *A broad-band method for measuring the complex permittivity of isotropic film-shaped materials at low microwave frequencies is presented. The characterized material is the substrate of an open-end microstrip line used as sample-cell. Complex permittivity is computed from S_{11} reflection parameter measurement of open-end microstrip cell using analytical relationships, which decrease the computation time. Vector network analyzer and high-quality on-microstrip test fixture are used for the measurement bench. Measurements over 0.01 GHz–3 GHz frequency range with several nonmagnetic materials show good agreements between measured and predicted results.* © 2007 Wiley Periodicals, Inc. Microwave Opt Technol Lett 49: 1371–1374, 2007; Published online in Wiley InterScience (www.interscience.wiley.com). DOI 10.1002/mop.22410

Key words: *microstrip line; permittivity broad-band measurement; radiofrequency and microwave; S*-parameters

1. INTRODUCTION

The necessity to characterize nonmagnetic film-shaped materials (ε_r) at low microwave frequencies (<3 GHz), has led us to develop a broad-band characterization experimental method. Among the different broad-band cells available in the literature [1–10], the microstrip and coplanar lines used as sample-cells adjust well to the characterization of film-shaped materials. Indeed, the measurements in free space require great dimensions of the samples to be characterized at these low microwave frequencies [1] and the measurements with box-shaped cells can become inaccurate, since they can present air-gaps between the conductors and the inserted sample [2–6]. The microstrip and coplanar cells allow changing its characteristic impedance to propagate the quasi-TEM mode and to perform accurate measurements, modifying the width of its conductor strip. The principal drawback of the microstrip and coplanar cells is the complexity to measure low-loss materials because of the metallic losses. However, the microstrip cell can allow a better concentration of the electric and magnetic fields into the dielectric substrate, and lower metallic losses than the coplanar cell.

The extraction methods associated to the microstrip and coplanar cells available in the literature do not conveniently measure the permittivity at low microwave frequencies (<3 GHz) [7–10]. Accurate results are obtained when the active part length of the cell is several integer multiple of one-half guided wavelength (λ_g) [11–12]. This is not always possible to be implemented when the frequency and the relative permittivity of the material are low. In this case, the use of a reflection method can be a solution. On the one hand, it provides information for the deduction of one complex parameter, either permittivity or permeability. In this work, we are interested in measuring electrical properties of nonmagnetic film-shaped materials. On the other hand, the properties of materials for a reflection method are fundamentally deduced from the cell admittance and the wave velocities in the cell and, therefore, the active part length of the cell does not usually come long. The unique reflection method based on microstrip line available in the literature uses a short-circuited microstrip line [13]. By contrast to this technique, an open-end microstrip line needs less technological processes, since it does not require via-hole between the strip and ground plane.

In this article, a reflection method is developed in order to satisfy the above requirements for the characterization of nonmagnetic film-shaped materials at low microwave frequencies (<3 GHz) and the restriction of the line length. The reflection method is based on an open-end microstrip line, which is used as sample-cell. The complex permittivity of the open-end microstrip substrate is extracted from S_{11} reflection parameter measurement, using a fast method based on analytical relationships, which takes into account the quasi-TEM mode. The measurements of open-end microstrip cells are carried out with a high-quality on-microstrip test fixture and a vector network analyzer covering 300 kHz–3 GHz.

2. MEASURING CELL AND MEASUREMENT BENCH

Two types of nonresonant methods can be used for the broad-band characterization of film-shaped materials with microstrip lines: transmission/reflection method and reflection method. The transmission/reflection method does not work well if the electrical length of the microstrip cell is lower than several integer multiples of one-half guided wavelength [9–12]. Thus, a reflection method